VLTI Imaging of a High-mass Protobinary System:

Unveiling the Dynamical Processes in High-mass Star Formation

Stefan Kraus

Jacques Kluska, Alex Kreplin, Matthew Bate, Tim Harries, Edward Hone,
Narsi Anugu (Exeter), Karl-Heinz Hofmann, Gerd Weigelt (MPIfR),
John Monnier (Michigan), Willem-Jan de Wit, Markus Wittkowski (ESO)

HansFest, Edinburgh
2018 September 6

Multiplicity in high-mass star formation

Multiplicity properties differ significantly for high-mass and low-mass stars:

➜ 80% of all O-stars are multiples, vs. 20% for solar-mass stars
(Chini et al. 2013)

➜ 2.5 companions/primary for Orion Trapezium stars, vs. 0.5 companions/primary for solar-mass stars

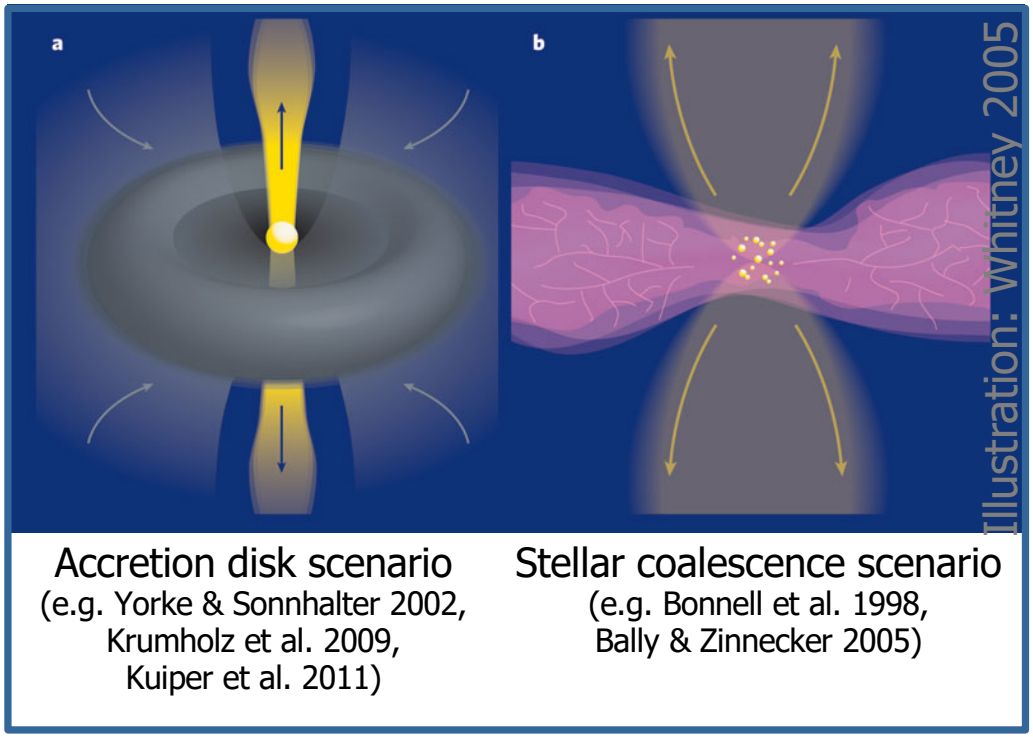

Accretion disk scenario
(e.g. Yorke & Sonnhalter 2002, Krumholz et al. 2009, Kuiper et al. 2011)

Stellar coalescence scenario
(e.g. Bonnell et al. 1998, Bally & Zinnecker 2005)

Possible formation mechanisms of high-mass multiples:

- Fragmentation in self-gravitating massive disks (Kratter & Matzner 2006)
- Disk-assisted capture (Clarke & Pringle 1991; Bally & Zinnecker 2005)
- Failed mergers in stellar collisions (Dale & Davies 2006)
- …

Previously imaged high-mass protobinaries

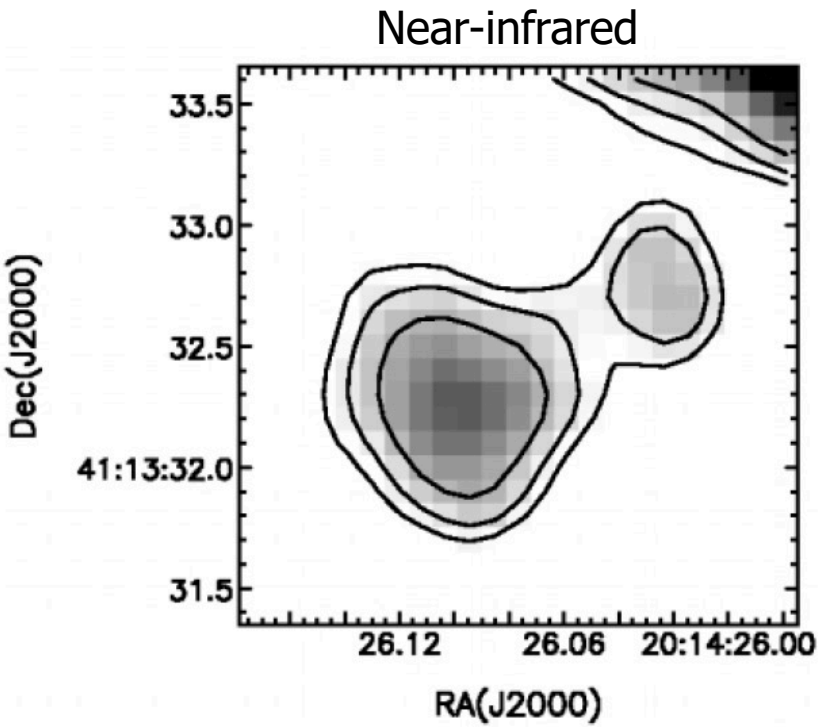

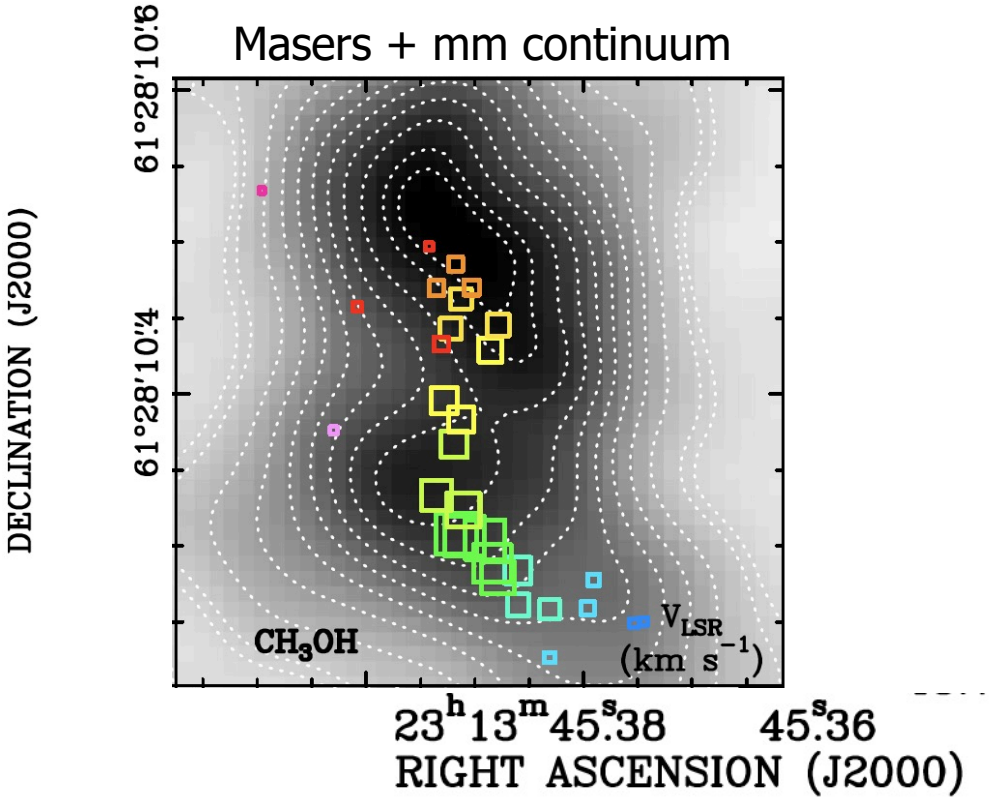

IRAS 20126+4104
System mass: ≈7 M_{sun}
Separation: 0.5″ = 850 AU
(Sridharan et al. 2005)

NGC7538 IRS1 a/b
System mass: ≈40 M_{sun}
Separation: 0.2″ = 500 AU
(Goddi et al. 2015)
(debated, e.g. Göran Sandell's talk)

➜ **Newly discovererd high-mass protobinary system:**
System mass: ≈40 M_{sun}
Separation: 0.058″ = 170 AU

Discovery of new high-mass protobinary system

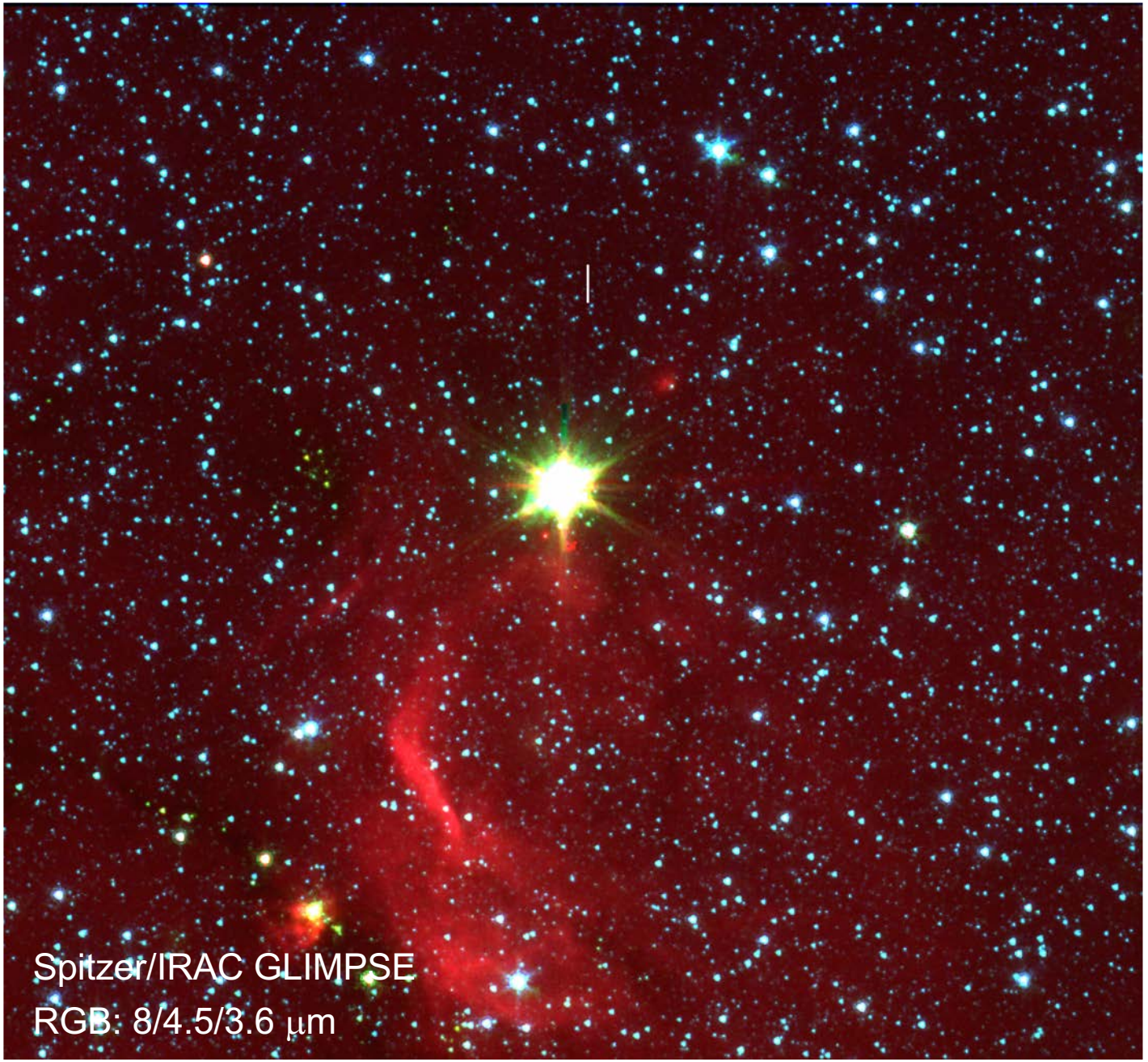

IRAS 17216-3801
High-mass YSO
Luminosity 61,000 $L_{\odot}$
Distance ~3000 pc

Observations

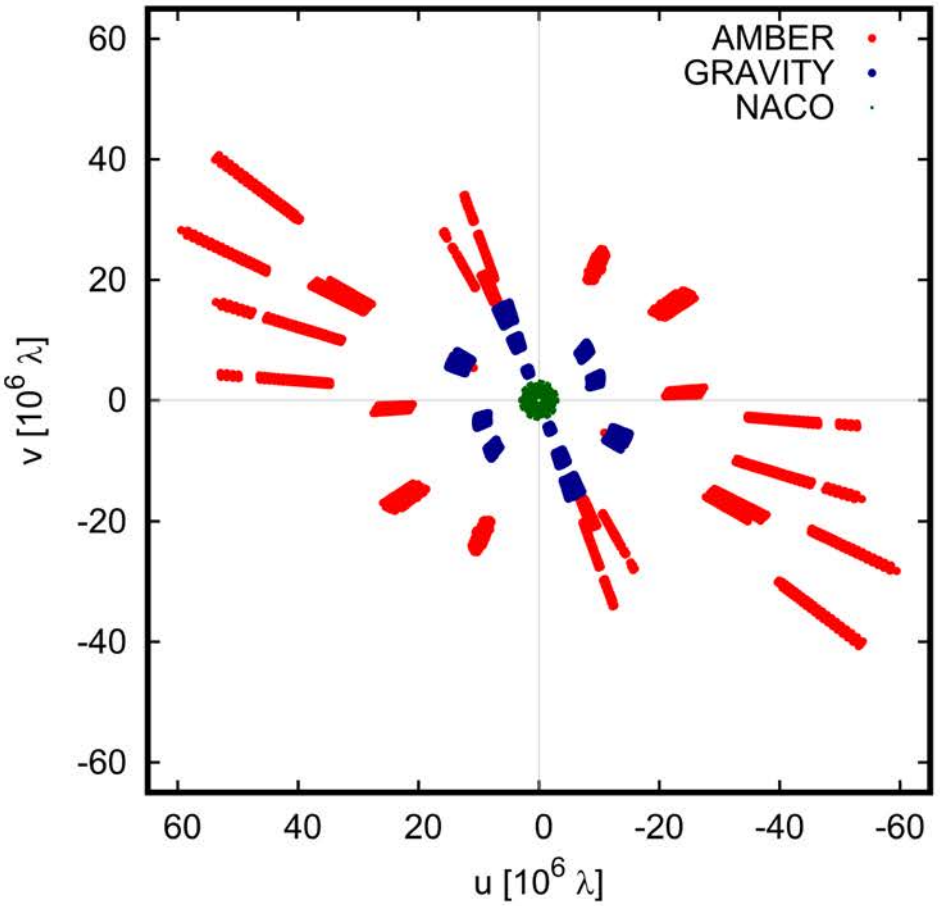

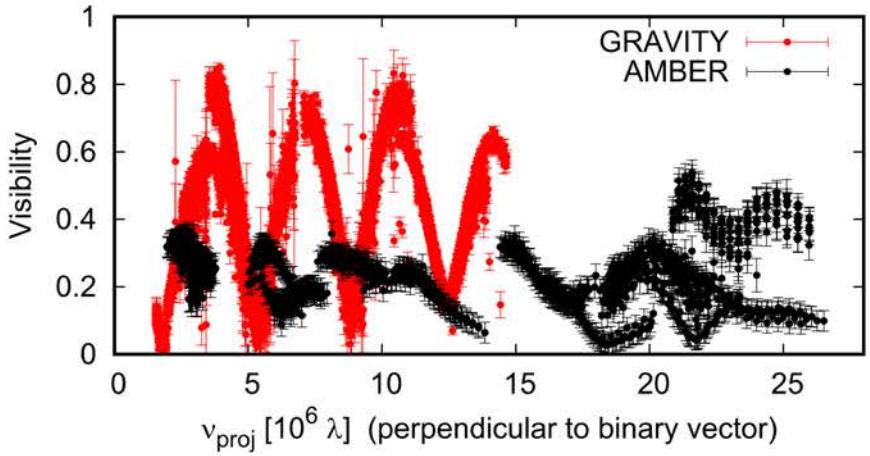

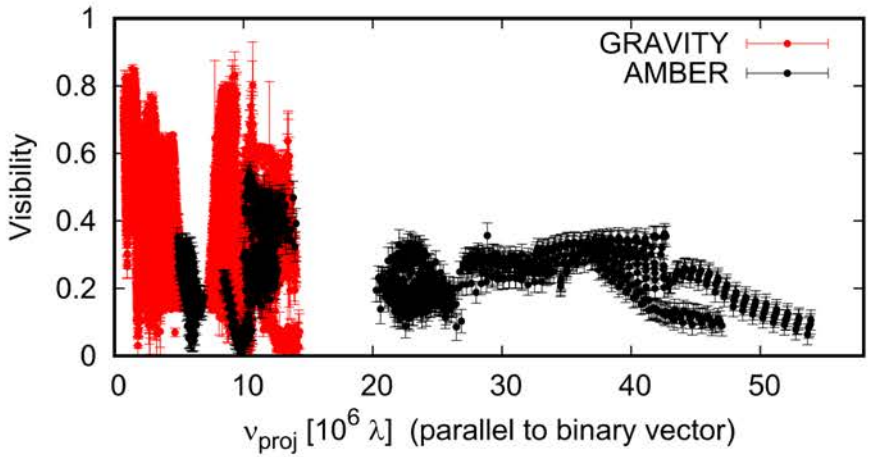

Dataset: 2012 VLTI/AMBER spectro-interferometry (R=35)
2012 VLT/CRIRES spectro-astrometry
2016 VLT/NACO imaging
2016 VLTI/GRAVITY spectro-interferometry (R=500)

Evaluating effects of temporal+bandwidth smearing

Observables show strong wavelength-differential modulation that changes on timescale of minutes

➜ **"Temporal" smearing:**
Split the data into subsets (bins of 50s, both for AMBER and GRAVITY)

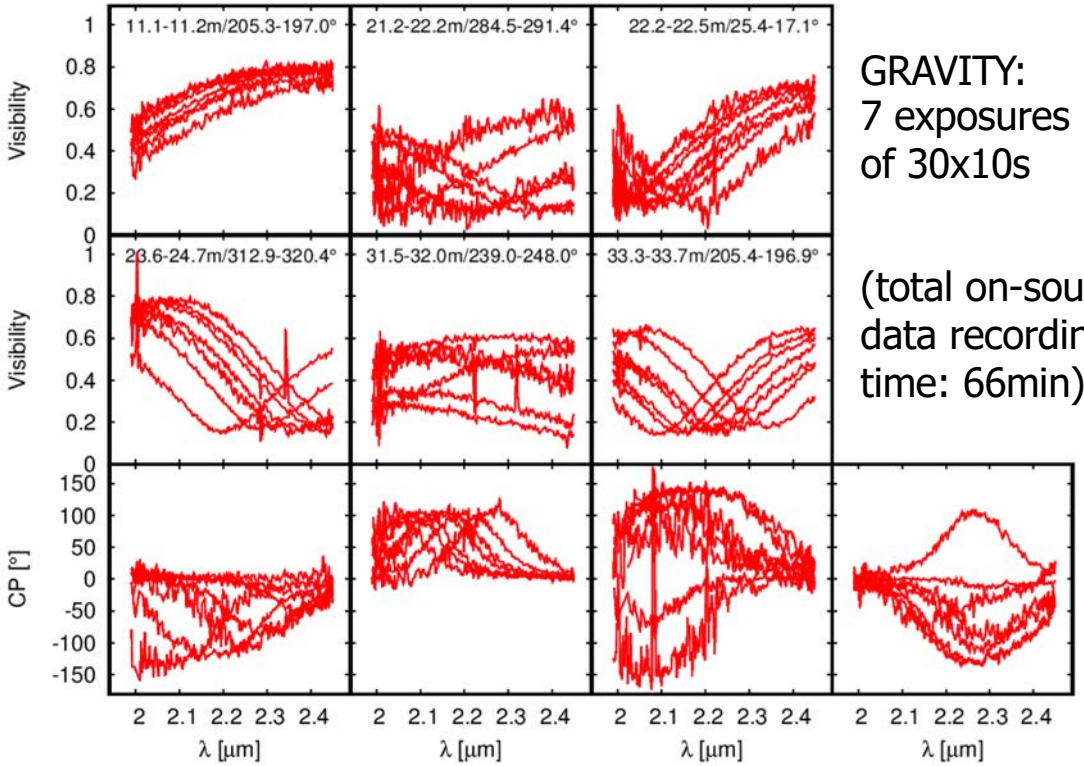

GRAVITY:
7 exposures of 30x10s

(total on-source data recording time: 66min)

$$c(\tau) = \frac{\sin\left(\pi\tau\Delta\lambda/\lambda^2\right)}{\pi\tau\Delta\lambda/\lambda^2}$$

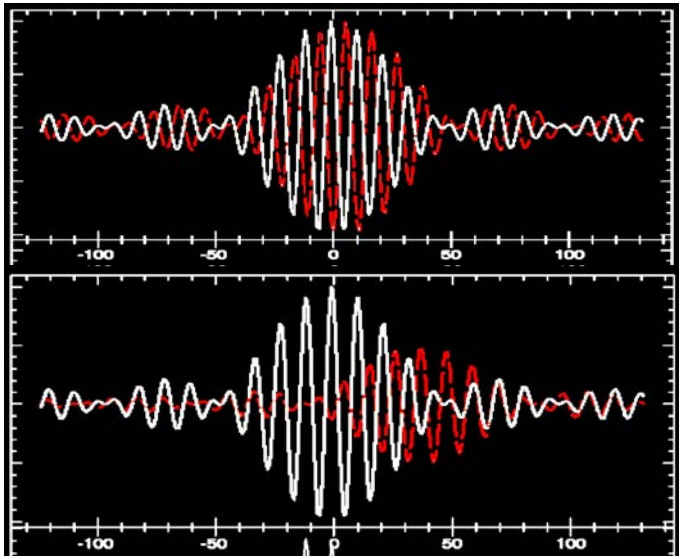

➜ **Bandwidth smearing:**

For wide-separation binaries, the phase difference between components can exceed width of coherence envelope, causing loss of coherence

AMBER (R=35): $\Delta c(\tau_{max}) \leq 2.5\%$

GRAVITY (R=500): $\Delta c(\tau_{max}) \leq 0.2\%$

GRAVITY+AMBER imaging

Aperture synthesis images, reconstructed using IRBIS algorithm (Hofmann et al. 2014)

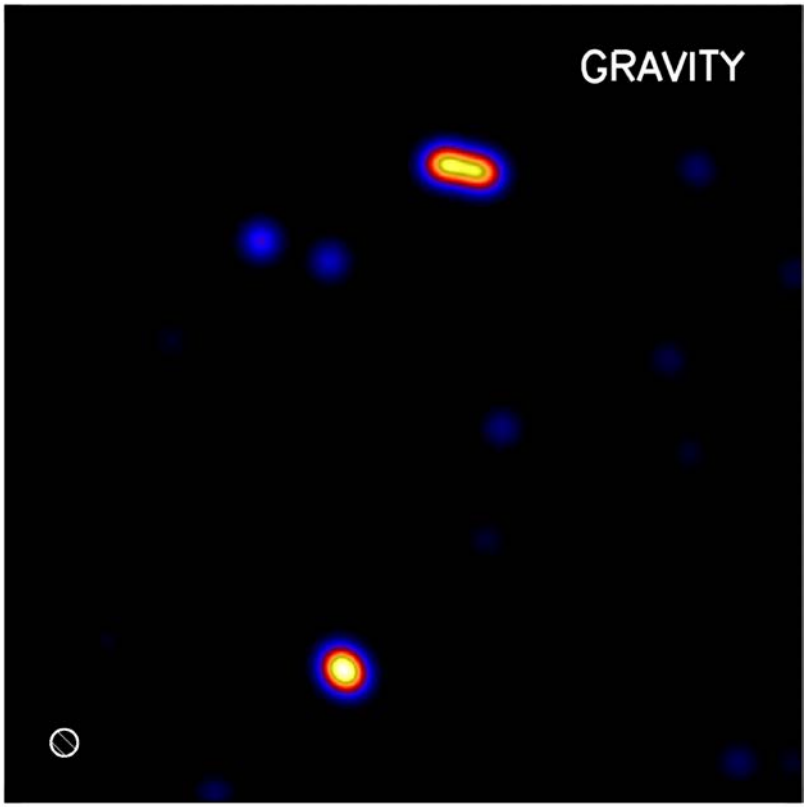

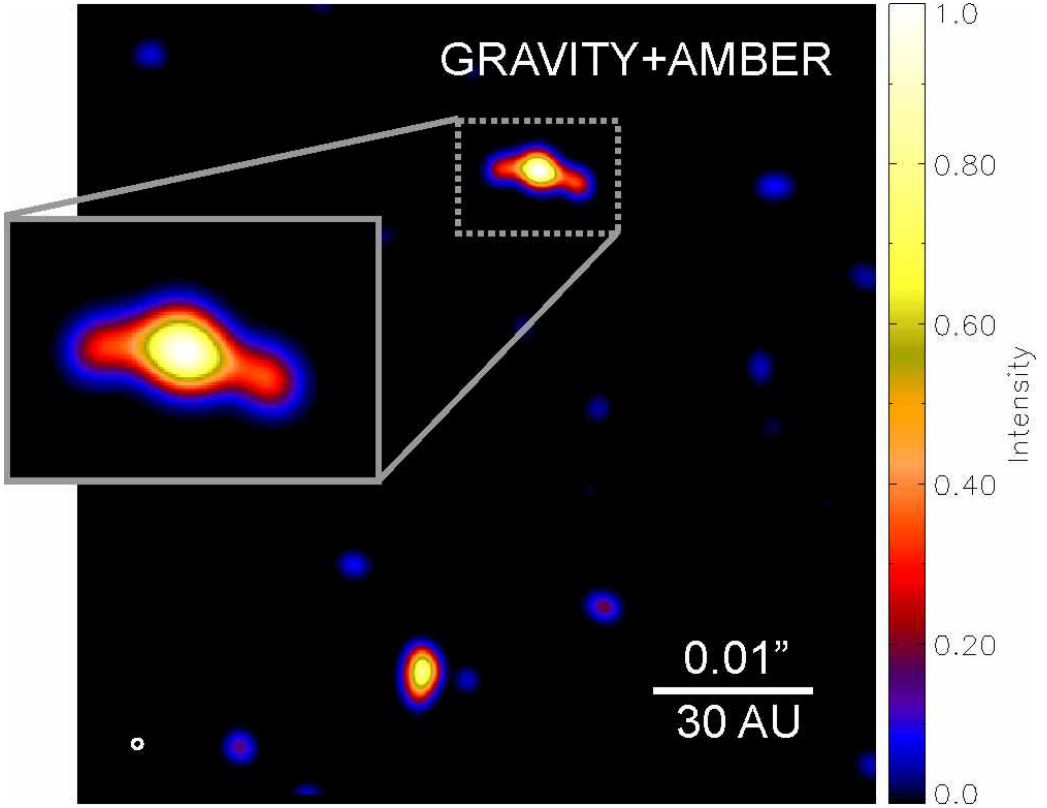

To compensate for orbital motion (2012 to 2016), we rotated/scaled the uv-plane synchronously to the system motion (Kraus et al. 2005)

Modelling

2 stars with disks + extended flux

assumed radial intensity profile:
GAUSS or temperature gradient DISK

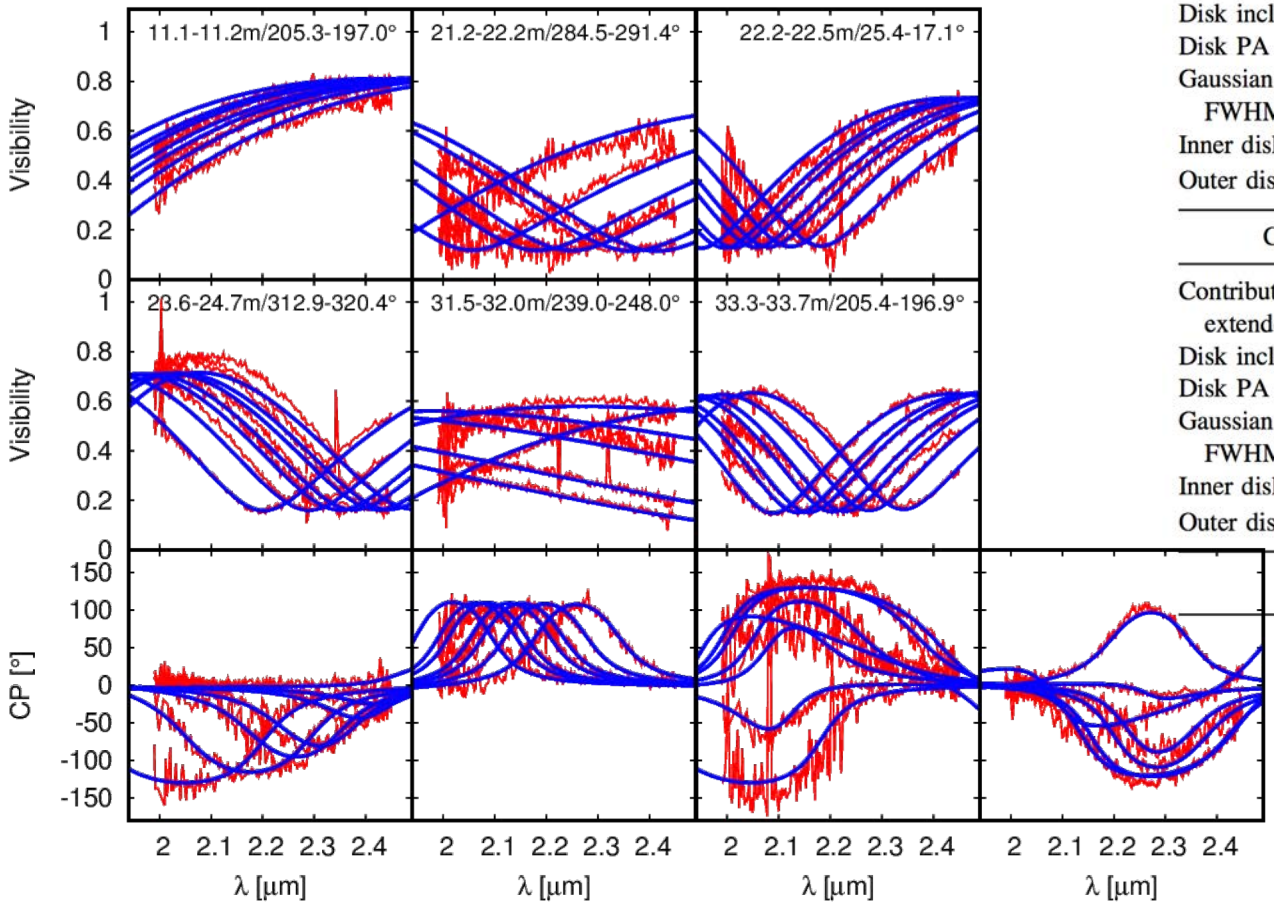

			GAUSS model	DISK model
Binary separation	ρ	(mas)	57.94 ± 0.24	57.93 ± 0.16
Binary PA	Θ	(°)	166.8 ± 0.2	166.76 ± 0.2
PA change 2012–2016	$\Delta\Theta$	(°)	7 ± 2	7 ± 2
Flux ratio	F_A/F_B		$1.29 \pm {}^{+0.09}_{-0.02}$	$1.26 \pm {}^{+0.13}_{-0.02}$
Extended flux contribution	F_{ext}/F_{tot}		0.16 ± 0.09	0.16 ± 0.06
Circumprimary Disk, Continuum (Northern Component, A)				
Contribution extended flux	F_A^{cs}/F_A		0.60 ± 0.08	0.64 ± 0.04
Disk inclination	i_A	(°)	89 ± 10	60 ± 10
Disk PA	θ_A	(°)	64 ± 9	67 ± 7
Gaussian FWHM size	Σ_A	(mas)	7.63 ± 0.8	…
Inner disk radius	r_A^{in}	(mas)	…	2.77 ± 0.39
Outer disk radius	r_A^{out}	(mas)	…	>12
Circumsecondary Disk, Continuum (Southern Component, B)				
Contribution extended flux	F_B^{cs}/F_B		0.90 ± 0.05	0.96 ± 0.09
Disk inclination	i_B	(°)	42 ± 7	38 ± 10
Disk PA	θ_B	(°)	185 ± 32	159 ± 15
Gaussian FWHM size	Σ_B	(mas)	4.60 ± 0.4	…
Inner disk radius	r_B^{in}	(mas)	…	2.49 ± 0.42
Outer disk radius	r_B^{out}	(mas)	…	>10
	χ_r^2		1.71	1.11

Modelling

Best-fit DISK model: T(r) ∝ r $^{-0.43}$

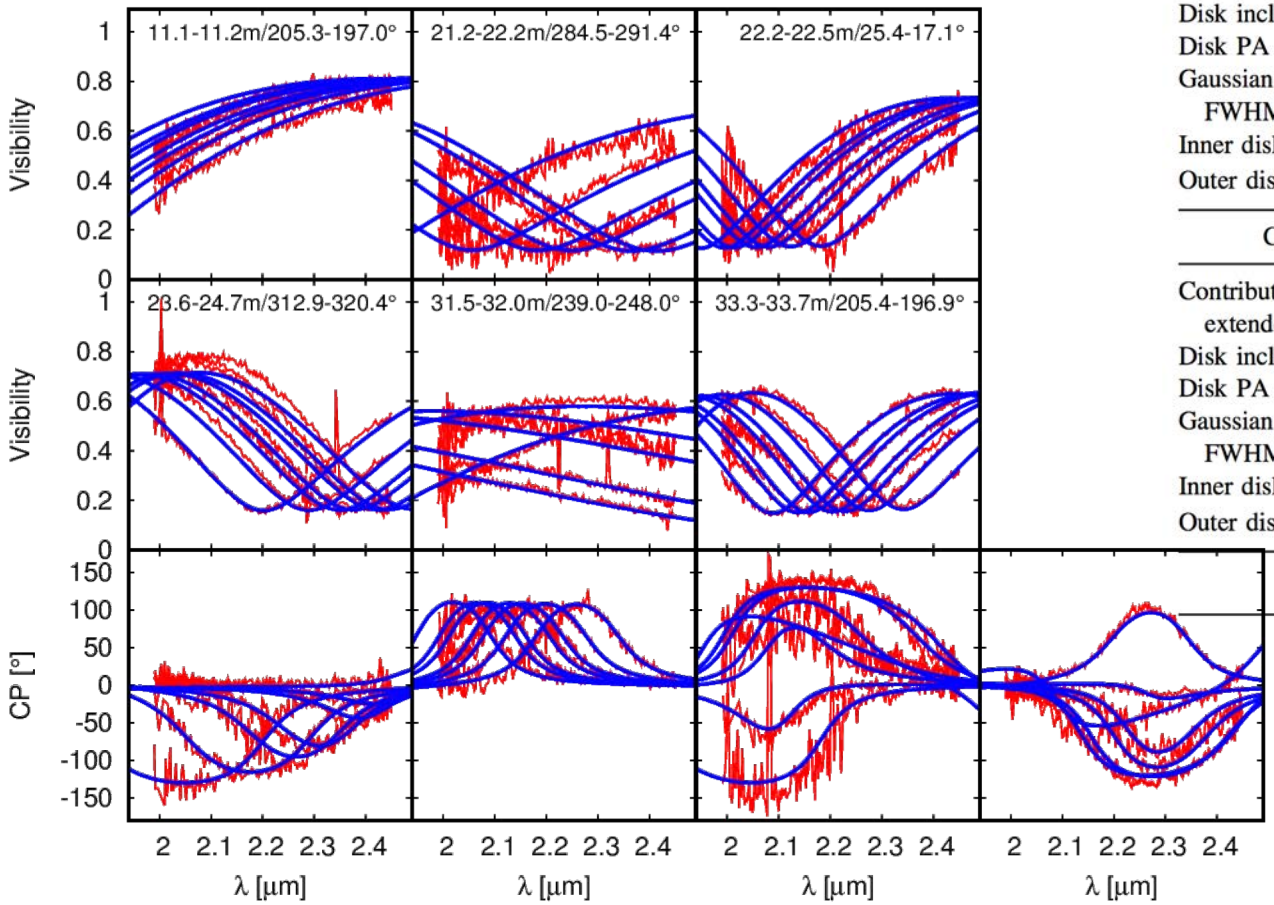

			GAUSS model	DISK model
Binary separation	ρ	(mas)	57.94 ± 0.24	57.93 ± 0.16
Binary PA	Θ	(°)	166.8 ± 0.2	166.76 ± 0.2
PA change 2012–2016	$\Delta\Theta$	(°)	7 ± 2	7 ± 2
Flux ratio	F_A/F_B		1.29 $\pm^{+0.09}_{-0.02}$	1.26 $\pm^{+0.13}_{-0.02}$
Extended flux contribution	F_{ext}/F_{tot}		0.16 ± 0.09	0.16 ± 0.06
Circumprimary Disk, Continuum (Northern Component, A)				
Contribution extended flux	F_A^{cs}/F_A		0.60 ± 0.08	0.64 ± 0.04
Disk inclination	i_A	(°)	89 ± 10	60 ± 10
Disk PA	θ_A	(°)	64 ± 9	67 ± 7
Gaussian FWHM size	Σ_A	(mas)	7.63 ± 0.8	…
Inner disk radius	r_A^{in}	(mas)	…	2.77 ± 0.39
Outer disk radius	r_A^{out}	(mas)	…	>12
Circumsecondary Disk, Continuum (Southern Component, B)				
Contribution extended flux	F_B^{cs}/F_B		0.90 ± 0.05	0.96 ± 0.09
Disk inclination	i_B	(°)	42 ± 7	38 ± 10
Disk PA	θ_B	(°)	185 ± 32	159 ± 15
Gaussian FWHM size	Σ_B	(mas)	4.60 ± 0.4	…
Inner disk radius	r_B^{in}	(mas)	…	2.49 ± 0.42
Outer disk radius	r_B^{out}	(mas)	…	>10
	χ_r^2		1.71	1.11

Modelling

Best-fit DISK model: $T(r) \propto r^{-0.43}$

Disks truncated at 8.6 and 7.7 au

➜ Consistent with dust sublimation radii for T=1300 K

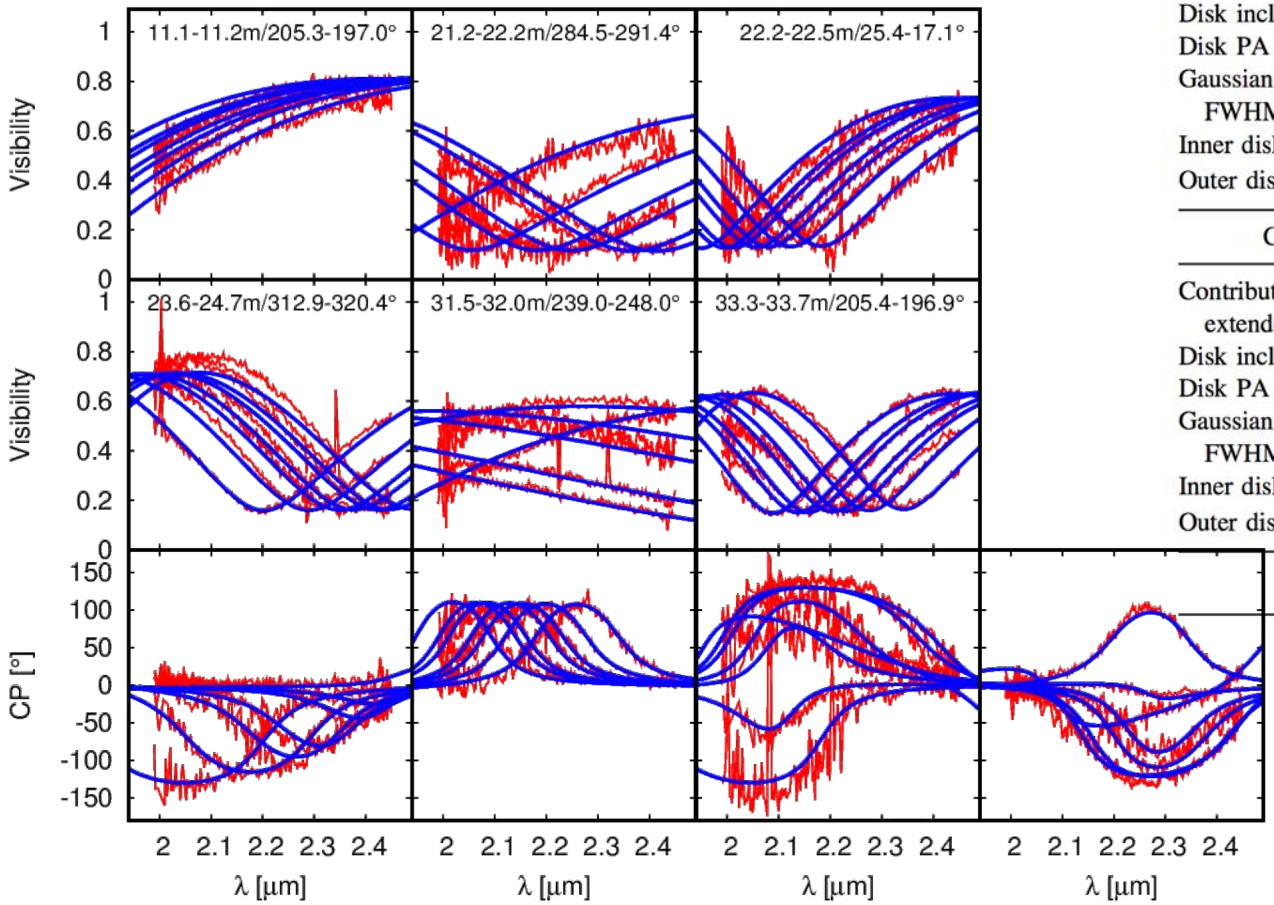

			GAUSS model	DISK model
Binary separation	ρ	(mas)	57.94 ± 0.24	57.93 ± 0.16
Binary PA	Θ	(°)	166.8 ± 0.2	166.76 ± 0.2
PA change 2012–2016	$\Delta\Theta$	(°)	7 ± 2	7 ± 2
Flux ratio	F_A/F_B		$1.29 \pm {}^{+0.09}_{-0.02}$	$1.26 \pm {}^{+0.13}_{-0.02}$
Extended flux contribution	F_{ext}/F_{tot}		0.16 ± 0.09	0.16 ± 0.06
Circumprimary Disk, Continuum (Northern Component, A)				
Contribution extended flux	F_A^{cs}/F_A		0.60 ± 0.08	0.64 ± 0.04
Disk inclination	i_A	(°)	89 ± 10	60 ± 10
Disk PA	θ_A	(°)	64 ± 9	67 ± 7
Gaussian FWHM size	Σ_A	(mas)	7.63 ± 0.8	…
Inner disk radius	r_A^{in}	(mas)	…	2.77 ± 0.39
Outer disk radius	r_A^{out}	(mas)	…	>12
Circumsecondary Disk, Continuum (Southern Component, B)				
Contribution extended flux	F_B^{cs}/F_B		0.90 ± 0.05	0.96 ± 0.09
Disk inclination	i_B	(°)	42 ± 7	38 ± 10
Disk PA	θ_B	(°)	185 ± 32	159 ± 15
Gaussian FWHM size	Σ_B	(mas)	4.60 ± 0.4	…
Inner disk radius	r_B^{in}	(mas)	…	2.49 ± 0.42
Outer disk radius	r_B^{out}	(mas)	…	>10
	χ_r^2		1.71	1.11

Modelling

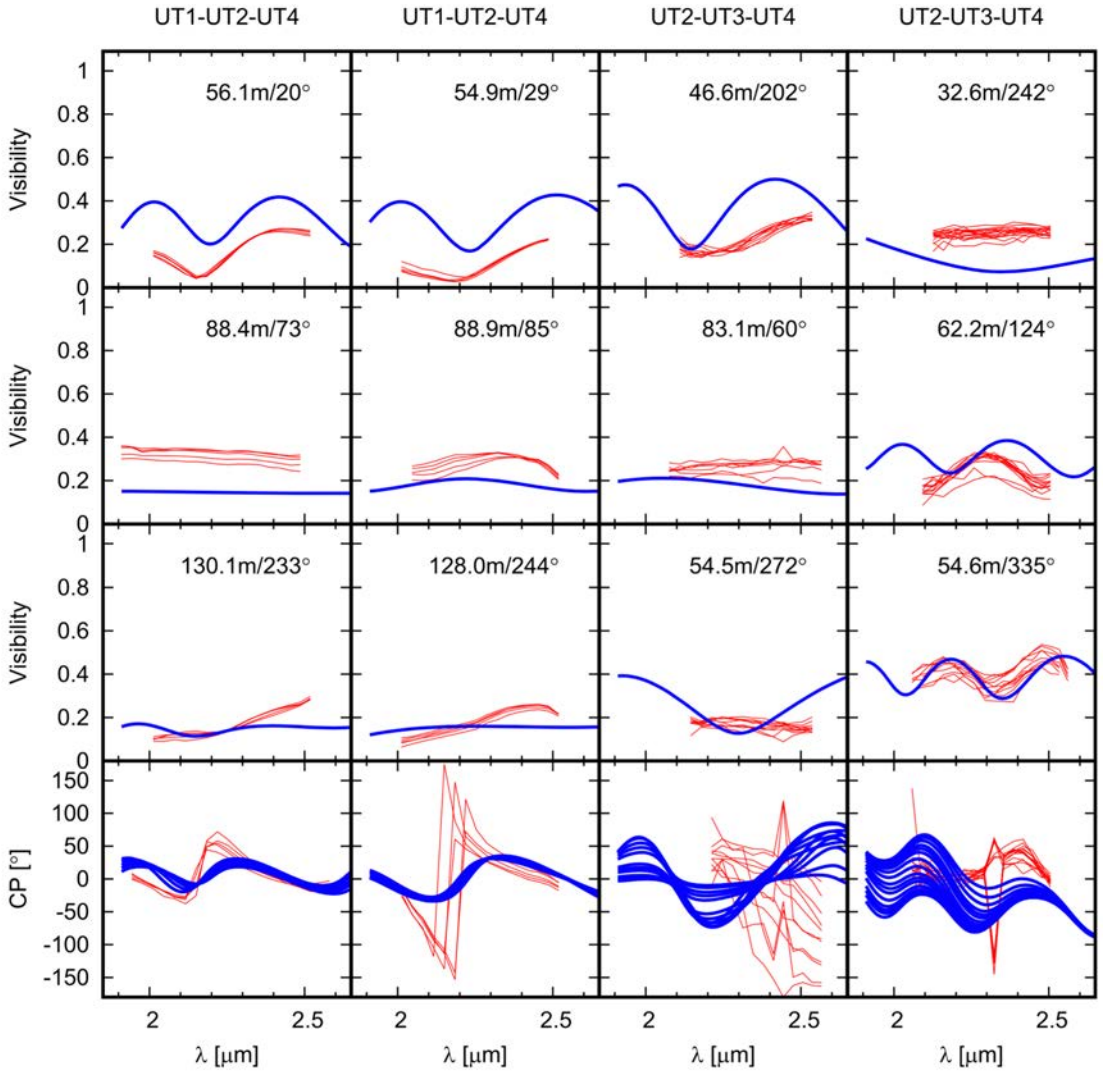

			GAUSS model	DISK model
Binary separation	ρ	(mas)	57.94 ± 0.24	57.93 ± 0.16
Binary PA	Θ	(°)	166.8 ± 0.2	166.76 ± 0.2
PA change 2012–2016	$\Delta\Theta$	(°)	7 ± 2	7 ± 2
Flux ratio	F_A/F_B		$1.29 \pm {}^{+0.09}_{-0.02}$	$1.26 \pm {}^{+0.13}_{-0.02}$
Extended flux contribution	F_{ext}/F_{tot}		0.16 ± 0.09	0.16 ± 0.06
Circumprimary Disk, Continuum (Northern Component, A)				
Contribution extended flux	F_A^{cs}/F_A		0.60 ± 0.08	0.64 ± 0.04
Disk inclination	i_A	(°)	89 ± 10	60 ± 10
Disk PA	θ_A	(°)	64 ± 9	67 ± 7
Gaussian FWHM size	Σ_A	(mas)	7.63 ± 0.8	…
Inner disk radius	r_A^{in}	(mas)	…	2.77 ± 0.39
Outer disk radius	r_A^{out}	(mas)	…	>12
Circumsecondary Disk, Continuum (Southern Component, B)				
Contribution extended flux	F_B^{cs}/F_B		0.90 ± 0.05	0.96 ± 0.09
Disk inclination	i_B	(°)	42 ± 7	38 ± 10
Disk PA	θ_B	(°)	185 ± 32	159 ± 15
Gaussian FWHM size	Σ_B	(mas)	4.60 ± 0.4	…
Inner disk radius	r_B^{in}	(mas)	…	2.49 ± 0.42
Outer disk radius	r_B^{out}	(mas)	…	>10
	χ_r^2		1.71	1.11

Dynamical history of IRAS17216 system

Sketch not to scale

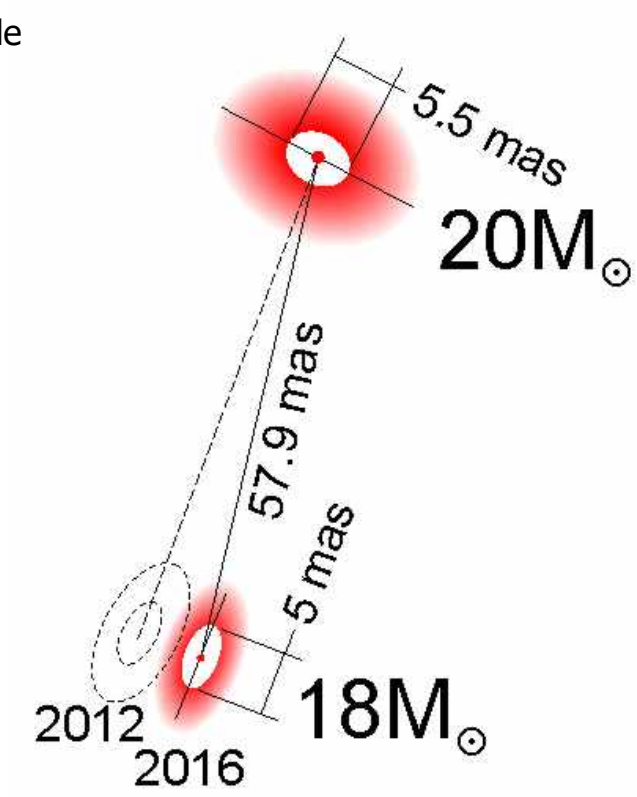

➜ **Circumprimary disk strongly misaligned w.r.t. binary separation vector**

Possible formation scenarios:

- Turbulent fragmentation
- Perturbation by a third component
- Star-disk capture
- Infall of material with angular momentum vector misaligned to gas that formed binary initially

Tidal forces work towards realigning disks w.r.t. orbital plane on precession timescale (< 200,000 yrs for circumprimary disk)

➜ **Tidal realignment is still ongoing, consistent with young dynamical age**

Strong misalignment of circumprimary disk

➜ **Weaker Lindblad torque that acts to truncate disk, explaining its larger extend**

Circumbinary disk

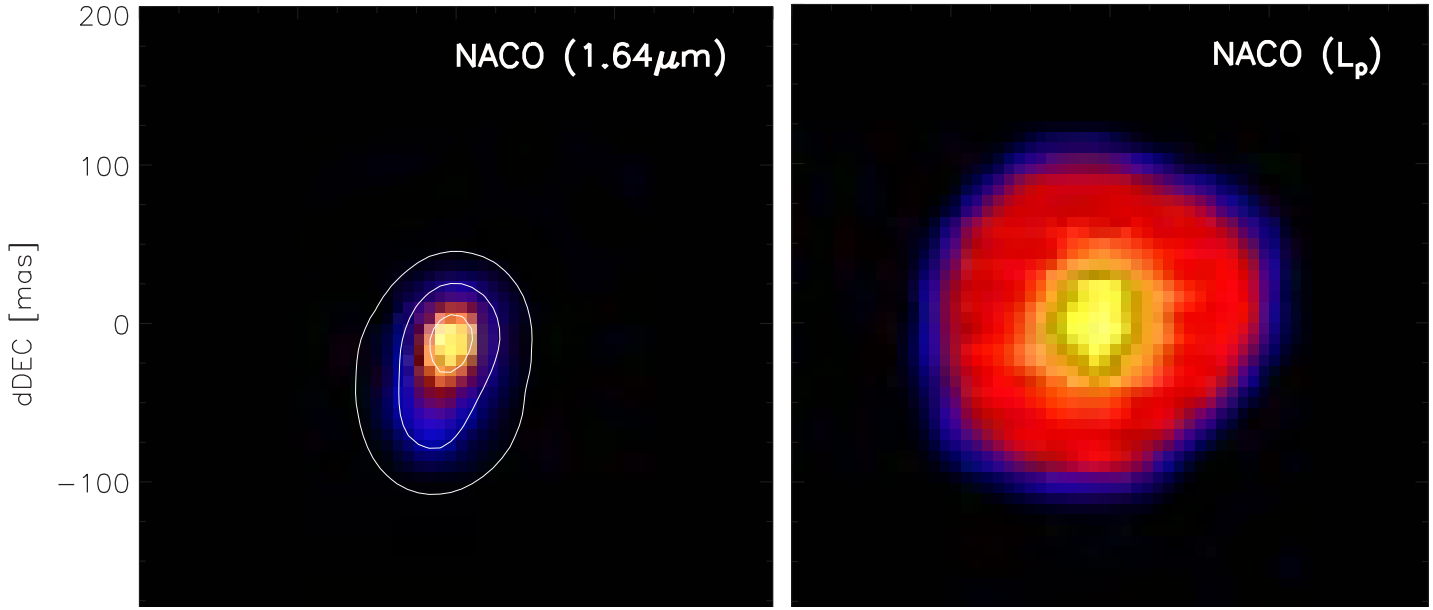

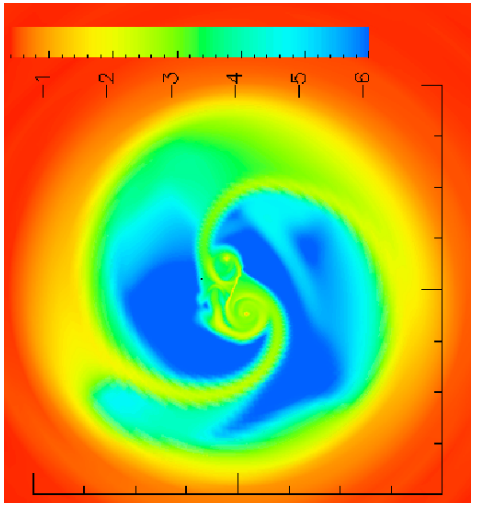

Binary disk truncation simulation
(Günther & Kley 2002)

NACO adaptive optics imaging:

J/H/K band (<2.1 μm):
Traces companion

L' band (3.8 μm):
Extended emission component
(4× larger than binary separation;
unfortunately, standard star missing)

➜ **Might trace thermal emission from inner edge of circumbinary disk**

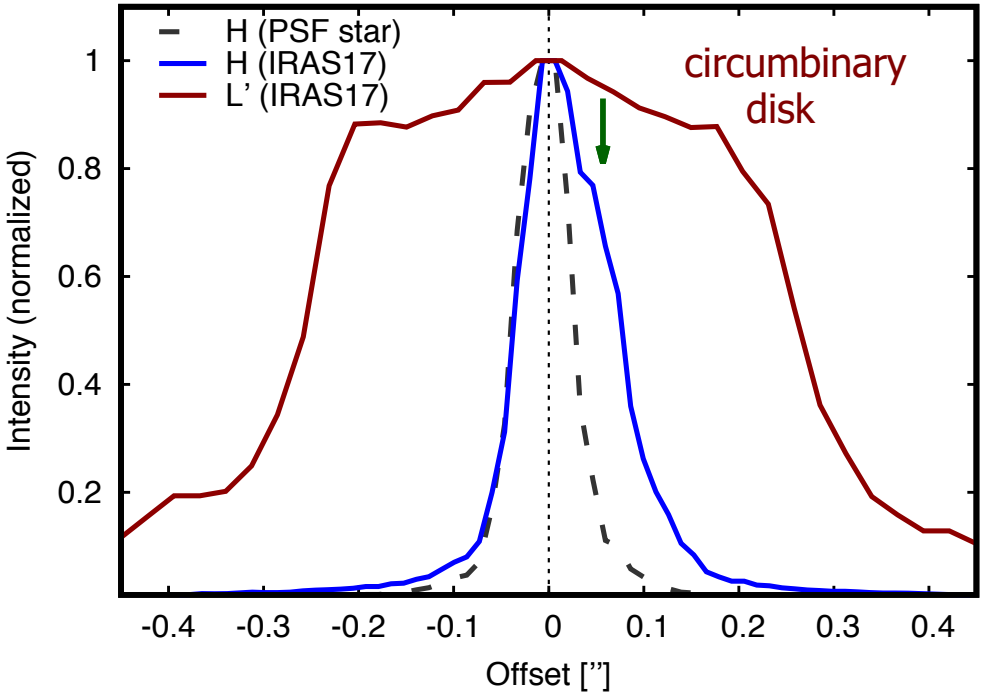

Accretion properties

CRIRES spectro-astrometry constrains origin of **Brγ hydrogen line emission**

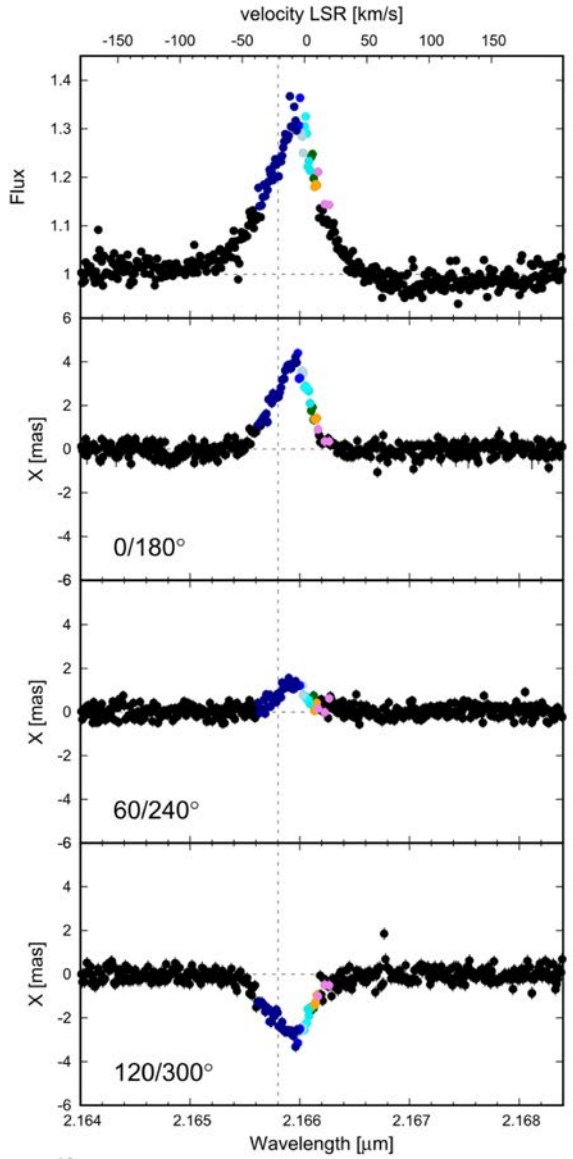

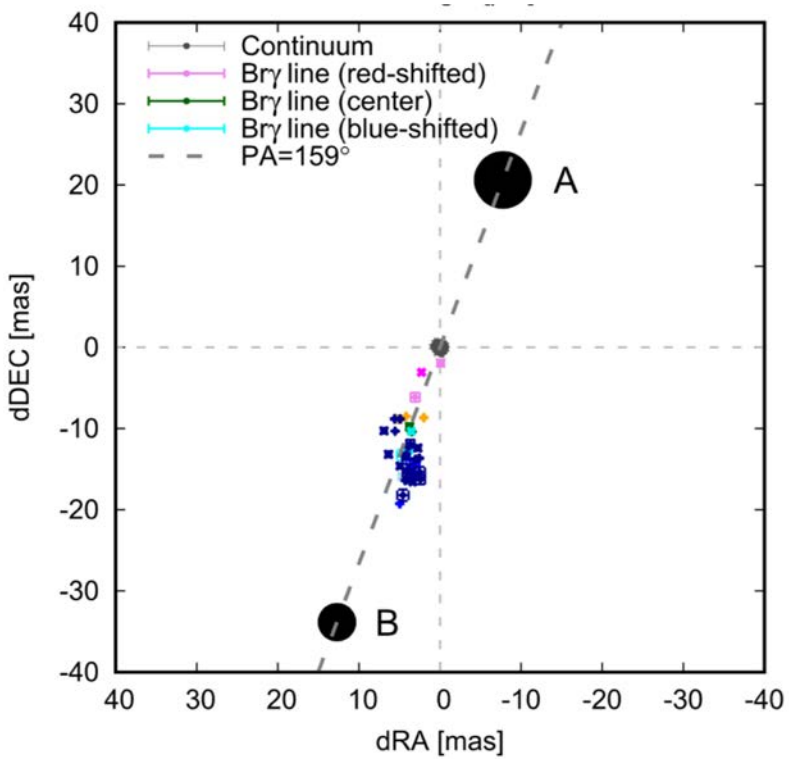

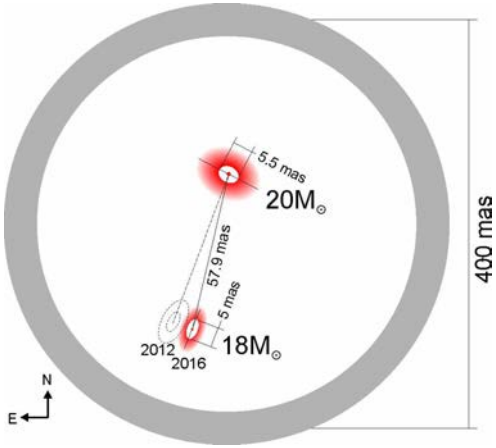

$$\frac{\dot{M}_B}{\dot{M}_A} = 1.6$$

➜ Secondary interrupts accretion stream onto primary, channeling most material onto circumsecondary disk (Whitworth et al. 1995; Bate & Bonnell 1997)

Brγ + CO bandhead emission

GRAVITY spectro-interferometry constrains origin of **Brγ + CO bandhead emission lines**

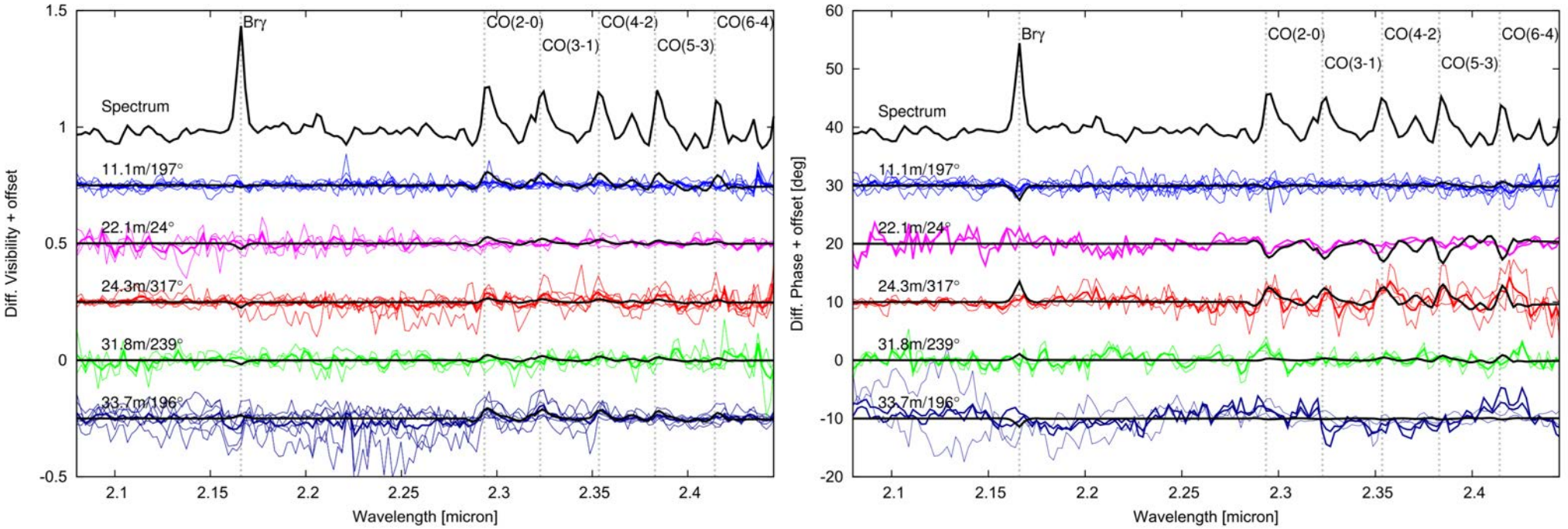

Brγ and CO bandhead emission originate from substantially different regions

Brγ: Unresolved emission at position of stars;
higher Brγ luminosity at position of secondary: $\frac{\dot{M}_B}{\dot{M}_A} = 1.5$

CO: Extended emission at position between stars (Gaussian FWHM 5.8 mas)

Conclusions

- GRAVITY+AMBER revealed **most compact protobinary system (170 AU)** imaged in thermal IR so far
- Orbital motion of 7±2° in 4 years ➜ **≈200 year orbital period**
- First system where **circumstellar disks** could be spatially resolved
- Circumprimary disk strongly misaligned w.r.t. binary separation vector
  ➜ **Tidal realignment is still ongoing**, consistent with young dynamical age
- **Secondary accretes at higher rate**, interrupting flow onto primary
- **CO bandhead emission** traces hot gas between stars

Reference:
Kraus et al.
(2017, ApJ 835, L5)